

The Locally Denatured State of Glutathione S-Transferase A1-1: Transition State Analysis of Ligand-dependent Formation of the C-Terminal Helix

Brenda S. Nieslanik, Eric C. Dietze, William M. Atkins
Department of Medicinal Chemistry
Box 357610
University of Washington
Seattle, WA 98195-7610
e-mail (WMA): winky@u.washington.edu

Isolde Le Trong, Ellie Adman
Department of Biological Structure
Box 357420
University of Washington
Seattle, WA 98195-7420

On the basis of available x-ray structures, A-class glutathione S-transferases (GSTs) contain at their C-termini a short α -helix that provides a 'lid' over the active site in the presence of the reaction products, glutathione-conjugates. However, in the ligand-free enzyme this helix is disordered and crystallographically invisible. An aromatic cluster including Phe-10, Phe-220, and the catalytic Tyr-9 within the C-terminal strand control the order of this helix. Here, preliminary x-ray crystallographic analyses of the wild type and F220Y rGSTA1-1 in the presence of GSH are described. Also, a transition state analysis is presented for ligand-dependent formation of the helix, based on variable temperature stopped-flow fluorescence. Together, the results suggest that the ligand-dependent ordering of the C-terminal strand occurs with a transition state that is highly desolvated, but with few intramolecular hydrogen bonds or electrostatic interactions. However, substitutions at Phe-220 modulate the activation parameters through interactions with the side chain of Tyr-9.

1. Introduction

The glutathione S-transferases (GSTs) catalyze the conjugation of the tripeptide glutathione (GSH; γ -glutamyl-cysteinyl-glycine) with an extraordinary range of drugs, toxins, and endogenous substrates. Collectively, the GSTs provide a major source of detoxification of xenobiotic electrophiles, and they play a critical role in the biosynthesis of prostaglandins (1, 2). Of particular interest is the overexpression of some GST isoforms in transformed cell lines and tumors, which accounts for GST-mediated resistance to many anticancer alkylating agents (3). Several gene classes of cytosolic GSTs have been identified in mammals, and they include A- (alpha), M- (mu), P- (pi), T- (theta), and K- (kappa) isoforms. Amino acid sequence homology between isozymes of different classes may be as low as 15 % depending on alignment parameters, but x-ray structures of representatives of each class in various ligand-states demonstrate a highly conserved overall topological fold (4 - 7).

Within this folded architecture, the N- and C-terminal domains contribute to a binding site that activates the nucleophile GSH by stabilizing the thiolate form, GS^- (8). This is achieved by a hydrogen bond to an active site Tyr or Ser (4 - 7).

A unique feature of the A-class GSTs is a C-terminal helix that provides a 'lid' over the active site in the presence of enzymatic product GSH conjugates. The x-ray structure of the human GSTA1-1 in the presence of the GSH ethacrynic acid conjugate, GS-EA, indicates that this helix must 'move or melt' in order for the product to dissociate. Moreover, in the absence of ligands, the structure of GSTA1-1 is essentially superimposable with the GS-EA bound protein. However, a striking difference between the structures is the absence of electron density corresponding to the C-terminal helix upon removal of the ligand due to local disorder. Indeed, the C-terminal 14 residues are crystallographically invisible in the apo-structure. A portion of the structure with GS-EA present is summarized in Figure 1, along with the relevant enzymatic reaction.

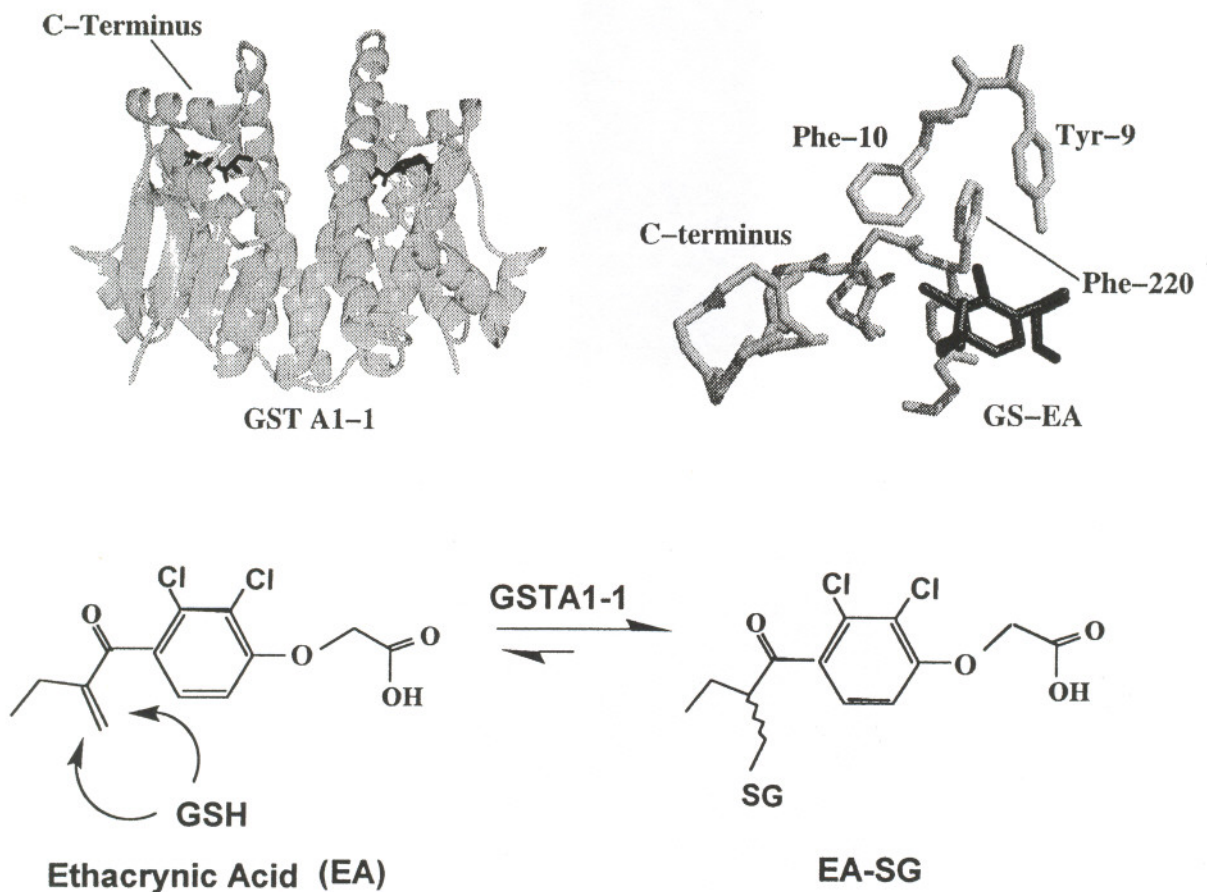


Figure 1. Top Left: Dimeric Structure of human GSTA1-1. The product GS-EA is bound at the active site in each subunit. The C-terminal helices restrict access to the active sites. Top Right: The active site region of GSTA1-1. Phe-220 within the C-terminal helix, Phe-10, and the catalytic Tyr-9 form an aromatic cluster that controls the order' of the helix. For clarity, only a portion of the GS-EA is shown. Upon removal of the ligand, the C-terminal helix affords poor electron density, and becomes crystallographically invisible. Bottom: GST-catalyzed formation of GS-EA from ethacrynic acid (EA).

Interestingly, the available structures indicate that the disorder \leftrightarrow helix transition must include a 'molecular switch.' Specifically, the completely conserved Phe-10 occupies the space directly above the aromatic ring of Tyr-9 in the absence of ligand. Electrostatic interactions between Phe-10 and the catalytic residue Tyr-9 contribute to the unusually low pKa of Tyr-9 in the apo-GSTA1-1 (10). In the GS-EA bound structure, Phe-10 has moved aside, and Phe-220 near the end of the C-terminal helix occupies the space above the Tyr-9 side chain. Thus, in the process of binding substrates and forming product conjugate, two specific changes occur: 1) Phe-10 moves away from Tyr-9 and 2) the C-terminal helix 'orders,' and replaces Phe-10 with the helix pendant Phe-220. However, detailed thermodynamic, kinetic, and structural characterization of this transition has not been performed previously.

Because product release is the rate limiting step for the majority of electrophilic conjugation reactions catalyzed by A-class GSTs (9), the disordered coil \leftrightarrow ordered helix transition is a critical determinant of the catalytic efficiency of these GST isoforms. In addition, the C-terminal helix of the GS-EA bound GST A1-1 communicates with the active site Tyr-9, to which GS⁻ is hydrogen bonded, and modulates the pKa of this catalytic residue. We previously have demonstrated with a combination of site-directed mutants, high pressure fluorescence spectroscopy, steady state kinetics, and *ab initio* calculations with small molecule models, that Phe-220 is a key player in the communication between the C-terminal strand and the active site in both GSH-bound and apo-forms of the enzyme (11, 12). On the basis of our previously published results from high pressure experiments, we envision that the C-terminal strand in the ligand-free state is analogous to a localized 'molten globule,' rather than a true random coil, and it samples a limited range of conformational space. However, the C-terminus lacks strong tertiary contacts with the remainder of the active site, and these contacts are required to form the catalytically competent ternary complex [GST • GS⁻ • Electrophile]. We and others have proposed that Phe-10 and Phe-220 control the conformational space that is sampled and the transition from the open, disordered, ensemble to the closed complex. In particular, we expect the F220Y mutant to have increased tertiary electrostatic interactions in the helical conformation.

In order to understand fully the molecular mechanisms that control this helix \leftrightarrow coil transition, we have initiated studies aimed at determining the x-ray structure of wild type and mutant GSTA1-1 variants in several ligand states, and performed transition state analysis to determine ΔH^\ddagger , ΔS^\ddagger , and ΔG^\ddagger for the association-dissociation reaction with the ligand GS-EA. This has been accomplished with temperature-dependent stopped-flow kinetic analyses. In addition, we have correlated the kinetic experiments with thermodynamic analyses for this ligand-dependent structural transition, with equilibrium fluorescence titration. We are currently validating the equilibrium measurements with isothermal titration calorimetry experiments, which yield ΔH° , ΔS° , and ΔG° directly.

As an additional probe of the C-terminal helix of GSTA1-1, we are in the process of determining the effects of the helix-inducing co-solvent trifluoroethanol (TFE) on the structure, turnover kinetics, and spectral properties of GSTA1-1 variants. As described within, low concentrations of this co-solvent specifically induce spectroscopic changes consistent with formation of the C-terminal helix, in the ligand-free GSTA1-1. In order to correlate these effects with structural changes, we have initiated crystal structure determination in the presence of TFE. Together, the combined experimental approaches described here are providing a detailed picture for the factors that control this localized structural transition.

2. Materials and Methods

2.1 Site-directed Mutagenesis, Protein expression, and Protein Purification.

Site-directed mutants of rGSTA1-1 were constructed and expressed in *E. coli*, as described previously (13). Briefly, mutant constructs were obtained by the PCR-based overlap extension method. Protein was expressed in *E. coli* strain DH5 α . For the studies described here, the mutant W21F is referred to as 'wild type.' This mutant was previously designed for spectroscopic purposes and exhibits behavior essentially identical to the true wild type. The x-ray structure included here verifies that this substitution has no effect on the active site or C-terminal helix.

2.2 X-ray Crystallography

Crystals were obtained in ammonium sulfate, Tris pH 8.5, 0.2M MgCl₂, and diffracted to 2.2Å on the laboratory R-axis. The space group was C222₁. Data processing and refinement utilized DENZO and XPLOR.

2.3 Stopped-Flow Kinetic Analysis.

Stopped-Flow fluorescence was performed with a SLM 8100 spectrofluorimeter equipped with a SLM milliflow reactor. Intrinsic tryptophan fluorescence was monitored with excitation at 295 nm and emission at 335 nm, with 2 μ M GST in 50 mM MES, pH 6.5 at 14°C. The k_{on} was determined by fitting the time-dependent change in fluorescence intensity to the equation $I(t) = Ae^{-(k_{obs})t}$ at E-SG concentrations between 10 μ M and 40 μ M, where $I(t)$ is the fluorescence intensity at time = t after mixing. The recovered rate constants, k_{obs} , at each E-SG concentration were fit to $k_{obs} = k_{on}[E-SG] + k_{off}$. The k_{off} was also determined directly by diluting the pre-formed binary complex, [GST • E-SG], in solutions containing 2 μ M GST and 20 μ M E-SG with buffer containing 1 mM S-hexyl GSH as a trapping agent.

2.4 Fluorescence Titrations with Co-Solvents.

The pK_a of Tyr-9 was monitored as described previously (10). Blank spectra were recorded for each concentration of co-solvent and subtracted from protein spectra. Temperature was maintained at 25°C. Samples contained 5 μM GST in 50 mM MES, at pH 7.5.

3. Results

3.1 Background.

In order to correlate the C-terminal helix <---> coil transition with GST function and with available structural data, we have focused on the substrate ethacrynic acid, which is a commonly used in vitro GST substrate. X-ray structures of A-class GSTs in the presence of ligands other than EA or GS-EA have not been published. Also, it was necessary to identify the rate limiting step for turnover of EA by GSTA1-1. In previously published work (9), we have described the effects of the concentration of a solvent viscosogen on rate, and shown that for EA turnover, physical steps involving protein motion, rather than chemical steps involving bond formation, are rate limiting. In addition, the correspondence between the k_{off} values measured by stopped-flow and steady state turnover rates, described below, indicates that release of the product conjugate GS-EA is rate limiting. Therefore, EA provides an ideal probe for correlating structure, kinetics, and thermodynamics of the disorder <---> order transition for this system. Our working hypothesis is that mutations that stabilize the C-terminal helix will lead to decreased V_{max}, due to decreased k_{off}.

3.2 X-ray structure of the binary complex [GST • GSH].

In order to determine at which point during the assembly of the catalytic complex, [GST • GS⁻ • EA], the helix becomes ordered, x-ray structure determination has been initiated for the wild type and F220Y mutant in the presence of GSH. Data collection statistics for summarized in Table 1, for the two proteins. Refinement is proceeding, and a useful structure is already available for the wild type. The R-factor after refinement is 0.27.

A significant finding is that in the presence of GSH, the C-terminal helix is disordered, as in the ligand-free state, and Phe-10 occupies the space directly above the aromatic ring of Tyr-9. Electron density for the Phe-10 is shown in Figure 2, along with the positions of Phe-10 and Phe-220 in the GS-EA complex. These results indicate that the C-terminal helix does not become ordered until the ternary complex is formed, or perhaps in the transition state leading to GSH conjugate

formation. As pointed out above, the helix is maintained in the product-bound state, at least for this substrate/ligand.

Table 1: X-ray Data Collection Statistics

| Crystal | F220Y/W21F | W21F (GSTGC) | W21F (GSTC) | 0Y/W21F 20YC) |
|---|---------------|------------------------|----------------------|------------------|
| Cell Dimensions (Å) | | | | |
| a | 85.65 | 84.5 | 84.3 | 6 |
| b | 278.3 | 274.9 | 273.8 | .2 |
| c | 71.70 | 70.4 | 70.30 | 3 |
| additive | none | S-hexyl glutathione | none | exyl tathione |
| Temperature | room | -160° | -160° | 0° |
| Resolution (Å) ^a | 2.2 (2.3-2.2) | 2.0 (2.09- 2.00) | 2.09 (2.22- 2.09) | 8 (1.98-1.88) |
| R-merge ^a on I | 0.079 (0.059) | 0.070 (0.162) | 0.069 (0.58) | 50 (0.29) |
| $\langle I \rangle / \langle \sigma(I) \rangle^a$ | 7.8 (1.9) | 18.3 (4.4) | 11.7 (1.5) | 8 (2.3) |
| Completeness ^a | 0.74 (0.54) | 0.91 (0.69) | 0.94 (0.84) | 5 (0.45) |
| Unique Reflections ^a | 30735 (3300) | 53068 (4899) | 47982 (2736) | 09 (4452) |

^aValues in parentheses are for the highest resolution shell.

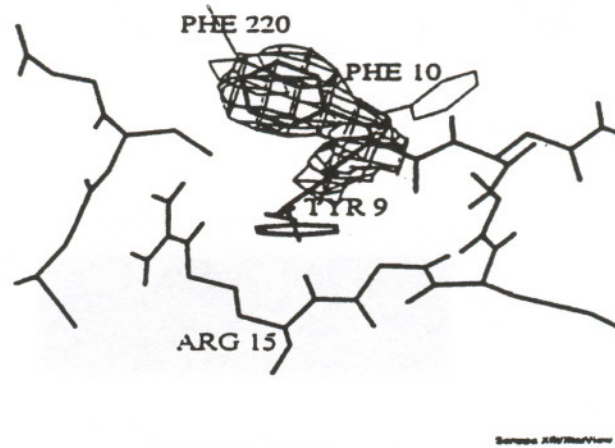


Figure 2. Electron density for Phe-10 in the binary, [GST • GSH], complex. Phe-10 sits directly above Tyr-9. Also shown are the positions of Phe-10 and Phe-220 when GS-EA is bound.

3.3 Transition state parameters for GS-EA binding to GSTA1-1's.

The rates k_{on} and k_{off} were measured by stopped-flow fluorescence, exploiting the ligand-induced changes in intrinsic fluorescence of the protein. For each mutant at each of the temperatures examined, the rate of approach to equilibrium after addition or dilution of ligand was adequately fit to a single exponential decay. Typical raw progress curves are shown in Figure 3, along with a plot of the concentration dependence of [GS-EA] on association rate, k_{obs} . The k_{on} and k_{off} , extracted from the analyses were also plotted at variable temperature, and these Eyring plots were used to obtain transition state parameters (Table 2).

The striking correlation that is apparent from these data is that mutations at Phe-220 which alter the off rate, k_{off} , also cause a nearly identical change in V_{max} . Also, the F220Y mutant exhibits a modest decrease in k_{off} relative to the wild type, but a more pronounced increase in k_{on} , which is ~4-fold faster than for the wild type. We have demonstrated previously, that the hydroxyl group of Tyr-220 is ideally situated to form a ($\pi \cdots \text{HO-Tyr}$) on face hydrogen bond in the GS-EA complex. This mutation is the only substitution with a natural amino acid that reduces the pK_a of GSH in the binary complex [GST • GSH]. Obviously, this mutation has the most pronounced effect on k_{on} .

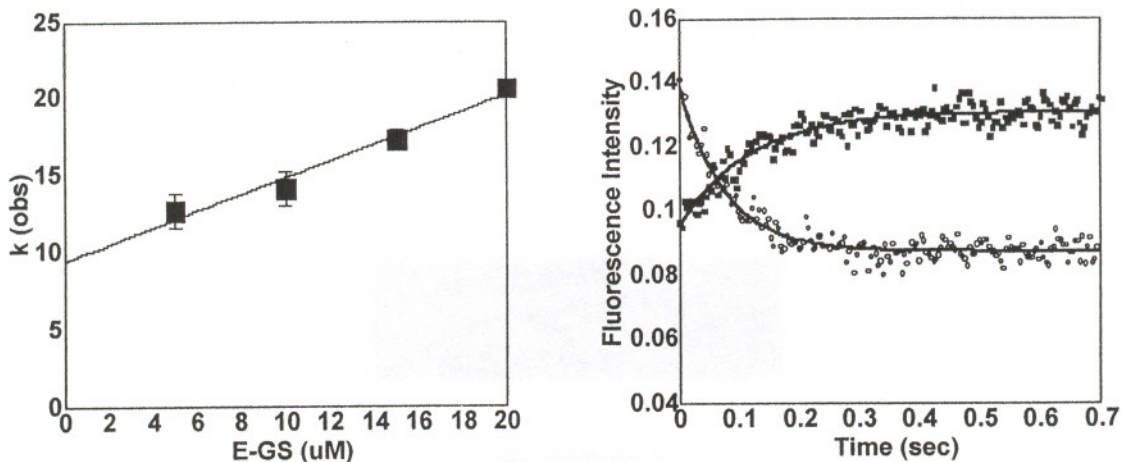


Figure 3. Left: k_{obs} vs. [GS-EA]. Right: Raw progress curves for association and dissociation of GS-EA with wild type GSTA1-1, obtained from stopped-flow fluorescence.

3.4 Equilibrium parameters for GS-EA association.

The equilibrium parameters for association of GS-EA were determined by fluorescence titration at a single temperature, 25°C . The recovered parameters are summarized in Table 2. Interestingly, the binding reaction for the wild type protein is entropically driven, suggesting that the ligand free state is highly solvated compared to the bound state. In comparison to the transition state parameter, ΔH^{\ddagger} , ΔH° for the wild type is significantly less positive, suggesting that the transition state has forfeited solvent-protein hydrogen bonds and electrostatic interactions without yet forming intrahelix or tertiary contacts. Also, the F220Y mutant exhibits an increase in the favorable contribution of ΔH° , consistent with additional electrostatic interactions between the newly incorporated hydroxyl group and the aromatic ring of Tyr-9, and a distinctly less favorable entropic change, upon reaching the complexed state. Presumably this reflects a more ordered, less solvated, state relative to the wild type in the ligand-free species. The results are of additional interest due to the entropy-enthalpy compensation that is apparent in the equilibrium parameters for wild type and F220Y mutant. Whereas ΔG° varies by only ~ 1 kcal/mol, the partitioning of the free energy of interaction with GS-EA is very different. Binding of this ligand to the wild type is entropically driven, whereas it is enthalpically driven for the mutant.

Table 2. Equilibrium and activation parameters for GS-EA binding to GST.

| parameter | wild type (W21F) | F220Y | F220I |
|---|---------------------|-------|-------|
| $k_{\text{cat}} (\text{s}^{-1})$ | 2.90 | 1.72 | 2.81 |
| $k_{\text{on}} (\mu\text{M}^{-1}\text{s}^{-1})$ | 0.24 | 0.88 | 0.37 |
| $k_{\text{off}} (\text{s}^{-1})$ | 1.87 | 1.26 | 1.88 |
| $K_{\text{d}} (\mu\text{M})_{\text{calc}}$ | 7.38 | 1.55 | 4.00 |
| $K_{\text{d}} (\mu\text{M})_{\text{exp}}$ | 4.47 | 1.75 | 2.71 |
| $\Delta H^{\ddagger}_{\text{a}}$ | 21.1 | 11.2 | 16.8 |
| $\Delta G^{\ddagger}_{\text{a}}$ | 10.3 | 9.2 | 9.5 |
| $T\Delta S^{\ddagger}_{\text{a}}$ | 11.1 | 1.9 | 7.3 |
| $\Delta H^{\ddagger}_{\text{d}}$ | 14.7 | 19.7 | 17.9 |
| $\Delta G^{\ddagger}_{\text{d}}$ | 16.8 | 16.9 | 16.7 |
| $T\Delta S^{\ddagger}_{\text{d}}$ | -2.1 | 2.9 | 1.1 |
| ΔG° | -6.8 | -7.8 | -7.2 |
| ΔH° | 0.4 | -6.7 | -1.0 |
| $T\Delta S^{\circ}$ | 7.2 | -1.0 | 6.2 |

$(K_{\text{d}})_{\text{calc}} = k_{\text{off}}/k_{\text{on}}$; $(K_{\text{d}})_{\text{exp}}$ is from fluorescence titration; $\Delta H^{\ddagger}_{\text{a}}$, $\Delta G^{\ddagger}_{\text{a}}$, $\Delta S^{\ddagger}_{\text{a}}$ are activation parameters for ligand association; $\Delta H^{\ddagger}_{\text{d}}$, $\Delta G^{\ddagger}_{\text{d}}$, $\Delta S^{\ddagger}_{\text{d}}$ are for dissociation; ΔG° , ΔH° , ΔS° calculated from activation parameters. Units for all activation and equilibrium parameters are kcal/mol.

3.5 Effects of Co-solvents on C-terminal Helix/Active Site Interactions.

The pKa of Tyr-9 was monitored by fluorescence spectroscopy as described previously. Briefly, Tyr absorbs maximally at 225 nm ($\epsilon = 8200\text{M}^{-1}\text{cm}^{-1}$) and 278 nm ($\epsilon = 1350\text{M}^{-1}\text{cm}^{-1}$). New absorbance bands are generated upon deprotonation

of the phenolic hydroxyl group at ~ 255 nm ($\epsilon = 11000 \text{ M}^{-1} \text{ cm}^{-1}$) and 295 nm ($2350 \text{ M}^{-1} \text{ cm}^{-1}$). In addition, the fluorescence emission is centered at 305 nm for protonated Tyr and at 340 nm for tyrosinate. The pKa of Tyr-9 in rGSTA1-1 is sufficiently below the pKas of other tyrosines to allow for its direct determination under variable conditions. The fluorescence intensities at 335 nm and 305 nm of various mutants with substitutions at Phe-220 were monitored with increasing concentrations of ETOH, DMF, or TFE. Concentrations as low as 5% TFE (v/v) markedly decrease the pKa of the catalytic Tyr-9 in the ligand-free enzyme, whereas ethanol or DMF at concentrations as high as 20% (v/v) induce no shift in this pKa. These results are consistent with the high pressure experiments (11). Furthermore, the sensitivity of the active site residue to TFE is dependent on the identity of the residue at position 220. Notably, the mutant F220Y, is least susceptible to TFE-induced helix formation. This, presumably, reflects the increased order of the helix in this mutant, relative to wild type or other mutants. We propose that TFE pushes the equilibrium ensemble of states toward the helix, in the absence of ligand. Mutants with increased thermodynamic driving force, such as an additional hydrogen bond in the F220Y mutant, require less TFE to afford this change in states.

4. Discussion

Together, past results and results presented here from ongoing experiments suggest an early transition state for the coil \rightarrow helix conversion, with a highly desolvated ensemble of structures with few tertiary electrostatic interactions or intrahelical hydrogen bonds. The TFE-specific decrease in the Tyr-9 pKa for all proteins other than the F220Y strongly suggests the formation of the C-terminal helix is responsible for the spectroscopic changes. This is consistent with the proposal that this mutant has a more ordered C-terminal helix in the apo-enzyme, as indicated by the transition state analyses. The combination of structural analysis, kinetic experiments and thermodynamic considerations are required to fully understand this functionally important change in the local order of these enzymes. The results demonstrate that the side chain at position 220 within the C-terminal helix is a critical determinant of the transition state structure leading to the functional ternary complex. In addition, it is interesting to speculate about the physiological role for local disorder in GSTs, and other proteins. For the case of GSTs, their physiological role requires a wide substrate diversity. Perhaps the locally disordered segment in the ligand-free GSTs is required to achieve plasticity in substrate binding.

Acknowledgments

This work was supported by the National Institutes of Health, GM51210.

References

1. Armstrong, R. N. Structure, catalytic mechanism, and evolution of the glutathione S-transferases. *Chem Res. Toxicol.* **10**: 2 - 18 (1997).
2. Mannervik, B. & Danielson, U. H. Glutathione S-transferases - structure and catalytic activity. *CRC Crit. Rev. Biochem.* **23**: 283 - 337 (1988).
3. Hayes, J. D. & Pulford, D. J. The glutathione S-transferase supergene family: regulation of GST and the contribution of the isozymes to cancer chemoprotection. *CRC in Biochem. and Mol. Biol.* **30**: 445 - 600 (1995).
4. Cameron, A. D., Sinning, I., L'Hermite, G. Olin, B., Board, P. G., Mannervik, B. & Jones, T. A. Structural analysis of human alpha-class glutathione s-transferase in the apo-form and on complexes with ethacrynic acid and its glutathione conjugate. *Structure* **3**: 717 - 727. (1995).
5. Ji, X., Armstrong, R. n. & Gilliland, G. I. Snapshots along the reaction coordinate of an S_NAR reaction catalyzed by glutathione S-transferase. *Biochemistry* **32**: 12949 - 12954 (1994).
6. Wilce, C. J., Board, P. G., Feil, S. C. & Parker, M. W. Crystal structure of a theta-class glutathione s-transferase. *EMBO J.* **14**: 2133 - 2143 (1995).
7. Reinemer, P., Dirr, H. W., Ladenstyein, R., Schaffer, J., Gallay, O. & Huber, R. The three-dimensional structure of class p glutathione S-transferase from human placenta in complex with S-hexyl glutathione at 2.8Å resolution. *J. Mol. Biol.* **227**: 214 - 226 (1992).
8. Graminski, G. F. & Armstrong, R. N. Spectroscopic and kinetic evidence for the thiolate anion of glutathione at the active site of glutathione S-transferase. *Biochemistry* **28**: 3562 - 3568 (1989).
9. Nieslanik, B. S. & Atkins, W. M. Contribution of linear free energy relationships to isozyme- and pH-dependent substrate selectivity: Comparison of model studies and enzymatic reactions. *J. Am. Chem. Soc.* **120**: 6651 - 6660 (1998).

10. Atkins, W. M. , Wang, R. W., Bird, A. W., Newton, D. J. & Lu, A. Y H The catalytic mechanism of glutathione S-transferase: Spectroscopic determination of the pKa of Tyr-9 in rat GSTA1-1. *J. Biol. Chem.* **268**: 19188 - 19191 (1993).
11. Atkins, W. M., Dietze, E. C. & Ibarra, C. Pressure-dependent ionization of Tyr-9 in glutathione S-transferase A1-1: Contribution of the C-terminal helix to 'soft' active site. *Prot. Sci.* **6**: 873 - 881 (1997).
12. Dietze, E. C., Ibarra, C., Dabrowski, M. J. Bird, A. & Atkins, W. M. Rational modulation of the catalytic activity of GSTA1-1: Evidence for an engineered on-face ($\pi \cdot \cdot \cdot \text{HO}$) hydrogen bond at Tyr-9. *Biochemistry* **35**: 11938 - 11944 (1996).
13. Wang, R. G., Newton, D. J., Pickett, C. B. & Lu, A. Y. H. Site-directed mutagenesis of glutathione S-transferase YaYa: Functional studies of histidine, cysteine, and tryptophan mutants. *Arch. Biochem. Biophys.* **297**: 86 - 91.